Received: 21 November 2018 | Revised: 14 April 2019 | Accepted: 20 May 2019

DOI: 10.1111/ffe.13072

SPECIAL ISSUE - NEW TRENDS IN FATIGUE AND FRACTURE - NT2F18

WILEY FFEMS Fatigue & Fracture of Engineering Materials & Structures

Fatigue crack propagation along interfaces of selective laser melting steel hybrid parts

Luis M.S. Santos[1] | José A.M. Ferreira[1] | Luis P. Borrego[1,2] | Jose D. Costa[1] | Carlos Capela[1,3] | Joel de Jesus[1]

[1] CEMMPRE, Department of Mechanical Engineering, University of Coimbra, Coimbra, Portugal

[2] Mechanical Engineering Department, Coimbra Polytechnic—ISEC, Coimbra, Portugal

[3] Mechanical Engineering Department, ESTG, Polytechnic Institute of Leiria, Leiria, Portugal

Correspondence
José A.M. Ferreira, CEMMPRE, Department of Mechanical Engineering, University of Coimbra, Coimbra P-3004 516, Portugal.
Email: martins.ferreira@dem.uc.pt

Abstract

Selective laser melting (SLM) is an emerging additive manufacturing technology, capable of producing complex geometry components. The current work studied both the effect of substrate material and mean stress on the fatigue crack growth behaviour along interfaces of bi-material specimens, substrate, and part by SLM. Fatigue tests were carried out in agreement with ASTM E647 standard, using 6-mm-thick compact specimens. The substrate steel has only a negligible effect both on the fatigue crack propagation rate and on the crack path. The failure occurs in the material additively manufactured by SLM, near the interface. The mean stress produced only a reduced influence on the fatigue crack propagation rate in the Paris regime. For larger values of ΔK, where K_{max} approaches K_{Ic}, a significant influence of the mean stress was observed. In spite of nondetection of crack closure, the application of overloads promoted significant fatigue crack retardation, quite similar for both substrate materials, probably due to the crack bifurcation during the overload.

KEYWORDS

additive manufacturing, compact (tension) specimens, crack paths, crack propagation, fatigue

1 | INTRODUCTION

Additive manufacturing (AM) processes produce components, directly from computer-aided design information, without the need of moulds or forming tools. In comparison with conventional manufacturing processes, AM allows raw material and manufacturing time savings and offer more freedom in design, which is an enabler for weight savings through topology optimization. Selective laser melting (SLM) produces mechanical components layer by layer, from a 3D model, by melting metal powder using a laser energy source. SLM offers the ability to generate highly customized parts for application in various industries,[1] but the presence of defects and microstructural heterogeneities creates uncertainty in their mechanical properties, making their widespread use difficult.[2] Moreover, high mechanical properties are required for many structural materials applications. Therefore, a significant research effort is still needed to better understand the mechanical behaviour of AM materials.

Nomenclature: AM, additive manufacturing; CPM, conventional powder metallurgy; *da/dN*, fatigue crack propagation rate; *N*, fatigue life; OLR, overload ratio; P_{op}, opening load; *R*, stress ratio; R^2, determination factor; SEM, scanning electron microscopy; SLM, selective laser melting; ΔK, stress intensity factor range; ΔK_{BL}, baseline stress intensity factor range before overload application; ΔK_{OL}, peak overload stress intensity factor range.

Material properties of SLM parts are also affected by residual stresses, internal defects, and the inherent roughness of the surface.[3,4] Recently, several conclusive studies[5-7] report the influence of different heat treatments and surface conditions on the tensile strength for SLM powder materials, while its influence on the fatigue behaviour[8] needs better understanding. The effect of different post-manufacturing heat treatments on the mechanical properties and microstructure was also studied by Rafi et al[9] and Facchini et al[10] for SLM 17-4 PH SS steel.

The manufacturing growing direction affects thermal history during fabrication and microstructure grain aspect ratio leading to an anisotropic behaviour of SLM materials. The loading direction in relation to the layer deposition plane also plays an important role on the mechanical properties of AM materials.[2] The influence of building orientation on tensile properties was confirmed by Luecke and Slotwinski[11] for the SLM 17-4 PH steel.

The fatigue behaviour of SLM components needs better understanding through more in-depth studies in order to obtain more reliable results and accurate predictions on fatigue design.[2] Recently, Mower and Long[12] and Yadollahi et al[13] studied the effect of building orientation on the fatigue behaviour of 17-4 PH steel.

The presence of pores in AM materials highly influences their fatigue behaviour. A significant number of studies were conducted in conventional powder metallurgy (CPM) materials reporting that crack initiation[14-16] and crack propagation[16,17] are influenced by porosity. In the presence of pore clusters, the interaction between pores usually occurs as a crack propagation mechanism.

According to Phillips et al,[18] the fatigue crack growth for several CPM steels is well predicted by a modified Paris growth law. They also concluded that the exponent of the Paris law during stable crack growth highly depends on the relative density, decreasing sharply to 2.6 to 4.0 when the full density is approximately achieved. In spite of the similarities of CPM and SLM processes in respect to typical porous, pore clusters and heterogeneous microstructure, fatigue crack growth in SLM materials have specific features.

No fatigue crack closure studies were found in SLM materials, contrary to conventional metals where fatigue crack growth is highly affected by plasticity at crack tip and consequently by the crack closure phenomenon.[19] For conventional metals, the crack closure approach generally permits to correlate the majority of the crack growth rate variations, after single overloads,[19-21] periodically applied overloads,[22] and two-level block loading, using experimental crack closure measurements.[23]

The present work intends to characterize fatigue crack propagation and failure mechanisms at both constant amplitude loading and transient regimes after overload application, for several stress ratios, in hybrid components with AISI 18Ni300 SLM steel built on three different substrate materials. Crack closure was monitored in all tests in order to investigate the eventual correlation with the stress ratio effect and crack growth rate variations after single overloads.

2 | MATERIALS AND EXPERIMENTAL PROCEDURE

Hybrid specimens were produced using conventional steel substrates over which were deposited the remaining part by selective laser melting (SLM). The SLM parts were manufactured in maraging steel AISI 18Ni300, while three steel substrates were used: the steel for hot work tools AISI H13, the stainless steel AISI 420, and a low-strength CK45E steel. The chemical composition and mechanical properties of these four materials are indicated in Tables 1 and 2, respectively.

Samples were manufactured using LaserCUSING technology, with layers growing in the same direction as the load application in the mechanical tests. The equipment for selective laser melting was the "Concept Laser," model "M3 Linear." This apparatus comprises a laser-type Nd:YAG with a maximum power of 100 W in continuous wave mode and a wavelength of 1064 nm. The samples were manufactured with a scan speed of 200 mm/s, adding layers of 30-μm thickness with hatch spacing of 100 μm and 25% overlapping, growing towards the direction corresponding to the application of load in the mechanical tests. After manufacturing, the specimens were ground on all surfaces, without post-heat treatment, and mechanically polished to facilitate optical observation of the crack during fatigue tests. Finally, the notch was performed by wire electrical discharge machining. Figure 1 shows schematically the building orientation where layer deposition plane is perpendicular to the loading direction.

Fatigue tests were carried out under sinusoidal load control, in agreement with ASTM E647[24] standard, using 6-mm-thick compact tension specimens (CT). Figure 2 shows the geometry and dimensions of the hybrid CT specimens, in which the direction of growth of the samples is in the test loading direction. All tests were carried out under load control and frequency of 10 Hz at room temperature using an Instron EletroPuls E10000 machine with 10-kN load capacity (Figure 3). The crack length was measured using a travelling microscope (45×) with an accuracy of 10 μm, as also shown in detail in Figure 3.

TABLE 1 Chemical composition of the materials (% wt)

Steel	C	Ni	Co	V	Mo	Ti	Cr	P	Si	Mn	Fe
18Ni300	0.01	18.2	9.0	-	5.0	0.6	0.3	0.01	0.1	0.04	Bal.
AISI 420	0.37	-	-	0.17	-	-	14.22	0.021	0.64	0.037	Bal.
AISI H13	0.4	-	-	0.94	1.30	-	5.29	0.017	1.05	0.036	Bal
CK45E	0.42	-	-	-	-	-	-	≦0.035	0.15	0.50	Bal

TABLE 2 Tensile properties of SLM material and substrate steels

Material	Yield Stress, MPa	UTS, MPa	Extension at Break, %
SLM material	1000	1147	6
AISI 420	1360	1600	12
AISI H13	1280	1520	12
CK45E	420	670	16

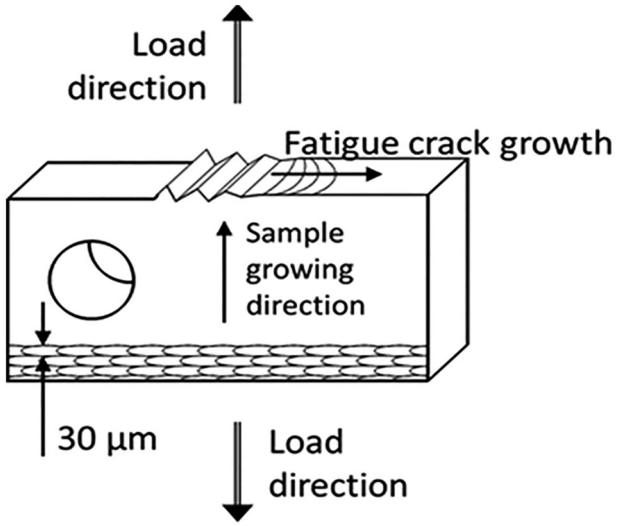

FIGURE 1 Sample building details

Crack growth rate under constant amplitude loading was determined by the incremental polynomial method using five consecutive points.[24] Figure 3 shows also a detail of the microgauge pin and its position in order to perform the measurements of crack closure loads.

The microstructure of the SLM material and interface zone of hybrid specimens were analysed according to the standard ASTM E407-99 of metallographic practice, performing a chemical attack with Picral (picric acid solution 4% in ethyl alcohol) during 2 minutes. After preparation, the microstructures of the samples were observed using a Leica DM4000 M LED optical microscope. Figure 4 shows the microstructures of the SLM part in Figure 4A and interface region for hybrid samples with AISI H13 and AISI 420 substrates in Figure 4B,C,

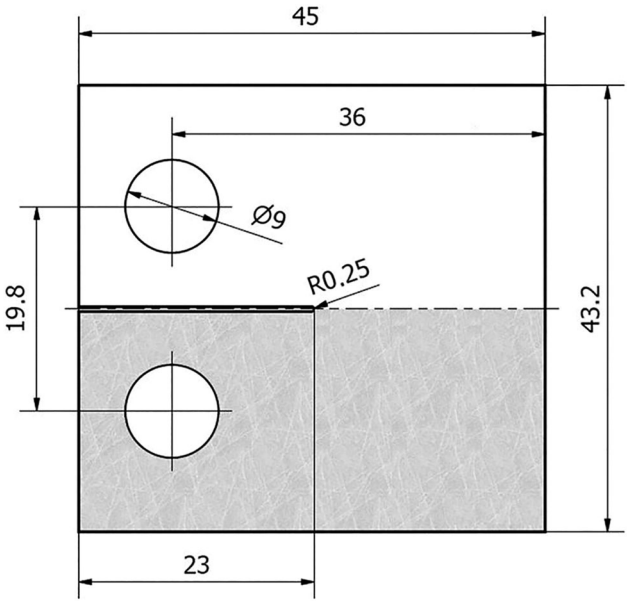

FIGURE 2 CT specimen dimensions (mm)

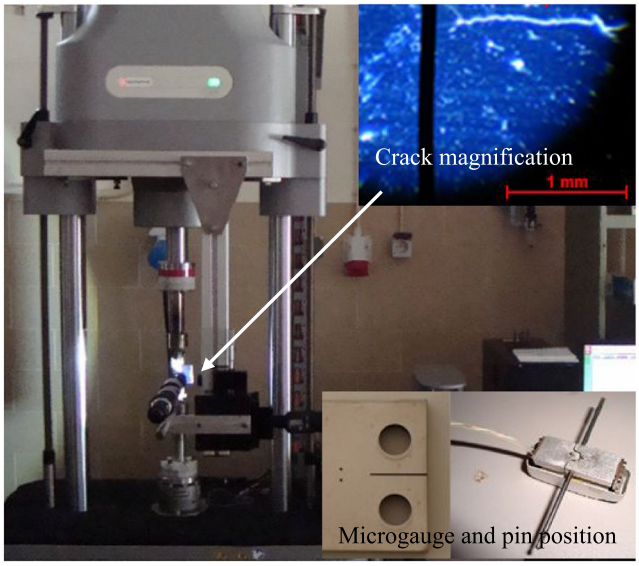

FIGURE 3 Testing machine and details of crack measurement, pin position, and crack closure measurement microgauge [Colour figure can be viewed at wileyonlinelibrary.com]

respectively. Figure 4A shows a typical SLM microstructure with elongated grains and martensitic regions. The substrate material shows a corrugated region created by

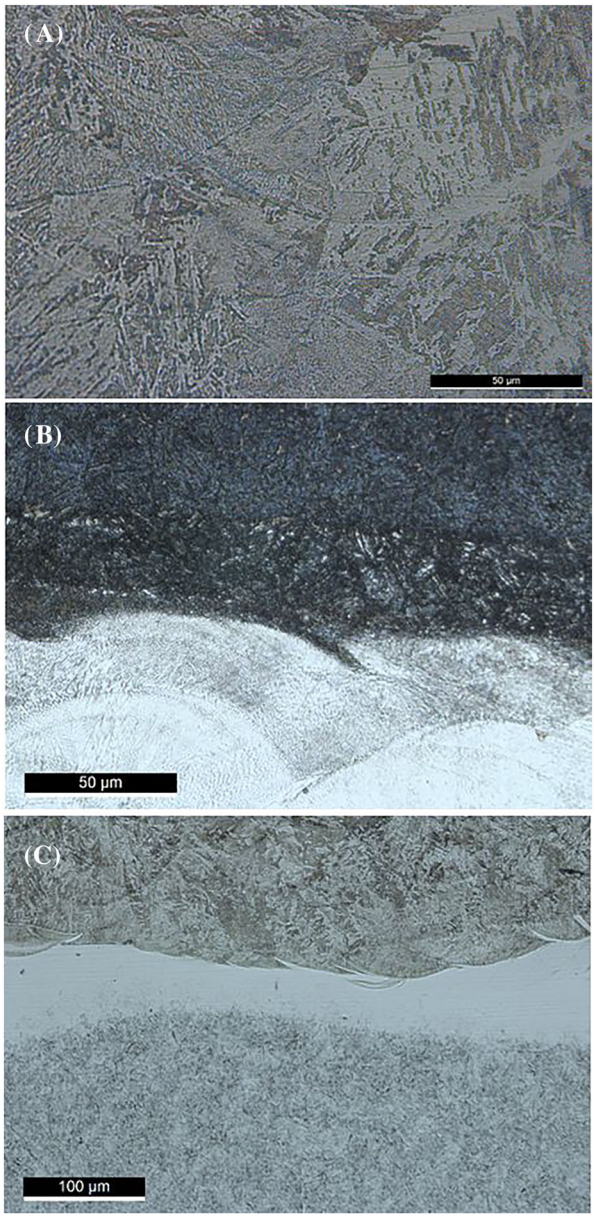

FIGURE 4 Macrostructure and microscopy observations of interface regions: A, SLM microstructure; B, interface for AISI H13 substrate; C, interface for AISI 420 substrate [Colour figure can be viewed at wileyonlinelibrary.com]

the melting in the first laser pass. A reduced formation of micro-pores was observed in the SLM part and also a transition between substrate and AM materials without the presence of lack of fusion zones. All the analysed samples presented the formation of lighter zones at the interface, resulting from the migration of carbon and consequently the occurrence of decarbonisation. In order to confirm these observations, the chemical analysis of the interface was performed on some specimens. Figure 5 compares the chemical composition at the interfaces of the hybrid samples with that of the SLM material, represented with an offset on the X-axis to make the graph

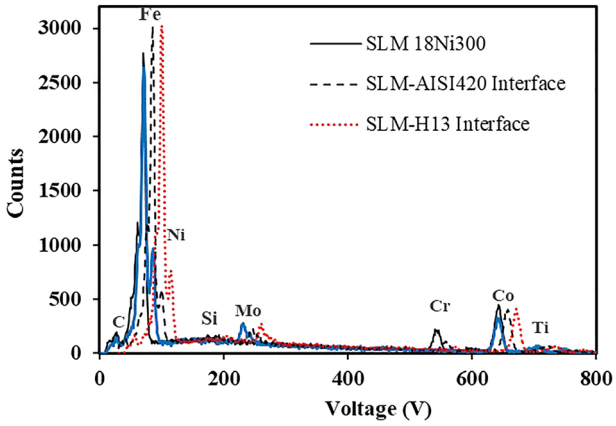

FIGURE 5 Chemical analysis on the interface for hybrid samples [Colour figure can be viewed at wileyonlinelibrary.com]

clearer. With the exception of Ni and Cr, the amounts of the remaining chemical elements are very similar in the three substrate materials, justifying the reduced influence of the substrate material on the results.

Vickers hardness was measured on the surface of the specimens in a line perpendicular to the interface using a Struers Duramin 1 microhardness tester with a 0.5-kg load and following the ASTM E384-11e1 standard. Figure 6 presents the hardness profiles for the three hybrid test samples with different substrate materials. This figure shows an average hardness of 340 HV for the SLM material, while for two of the analysed substrates, a much higher hardness was obtained, 530 HV in the AISI420 and 510 HV in the AISI H13 and a much lower hardness of 180 HV in the CK45 steel. The interface zone presents intermediate values of hardness between the subtract and the SLM materials.

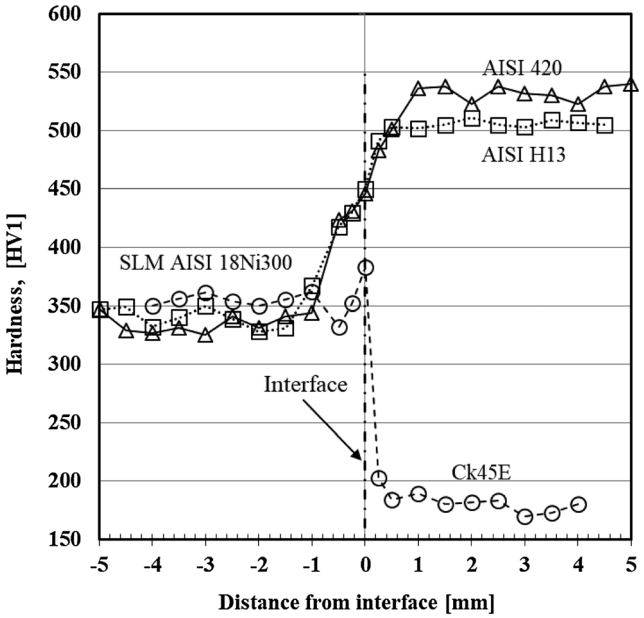

FIGURE 6 Hardness profiles around the interface region

Residual stresses are one of the main factors that affect fatigue performance of selective laser-melted materials. Residual stress analysis was performed by X-ray diffraction using a Proto iXRD equipment. Figure 7 presents the mean values and standard deviation of the longitudinal stress (y-axis in Figure 1) in a region close to the surface of the SLM material at coordinates x = 5 and y = 1.5 mm. These results show that the residual stresses decrease with the distance to the surface, having a tensile stress with a mean value of 220 MPa in a 200-μm surface layer and stable values of the diffraction peak breadth around 4.05°. As the residual stresses were measured in only one position of the SLM material and close to the surface, it is impossible to carry out a conclusive discussion on its influence on the crack propagation rate during constant amplitude load tests and during the transient regime after the application of overloads. For this, it would be necessary to obtain a complete characterization of the residual stresses both in the direction of the z-axis, up to half thickness, and in the direction of crack propagation of the crack (x-axis in Figure 1), which was outside the objectives to be achieved with this work.

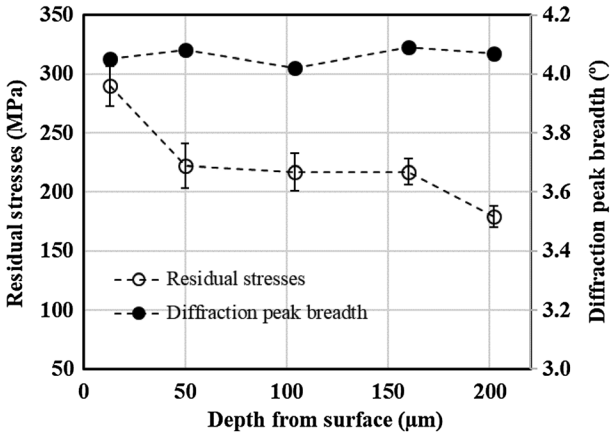

FIGURE 7 Profile of the longitudinal (loading direction) residual stresses

The influence of tensile overloads was investigated in the Paris regime at $R = 0.05$. Single and multiple tensile overloads were also performed under load control, with a ΔK baseline level (ΔK_{BL}) of 12 and 18 MPa$\sqrt{m}$. The overload ratio, defined as,

$$OLR = \frac{\Delta K_{OL}}{\Delta K_{BL}}, \quad (1)$$

was OLR = 2, where ΔK_{OL} and ΔK_{BL} are the peak overload stress intensity factor range and the baseline stress intensity factor range before the overload application, respectively. Therefore, each overload was applied with 100% increase in load, respectively, to the baseline loading range.

Load-displacement curves were monitored at specific crack length increments throughout each of the tests using a pin microgauge elaborated from a high sensitive commercial axial extensometer (±0.625 mm of maximum displacement). As showed also in Figure 3, the gauge pins were placed at the centre of the specimens in two drilled holes of 0.5-mm diameter with 3.5-mm distance between them. Load-displacement data acquisition was done after the crack advances beyond the pins. Data collection was performed at a reduced frequency of 0.5 Hz. Table 3 summarizes all fatigue tests that were performed indicating the loading parameters used.

The fracture surface analysis was performed with a scanning electron microscope Philips XL30.

3 | RESULTS AND DISCUSSION

3.1 | Crack propagation under constant amplitude loading

Mechanical properties of the SLM AISI 18Ni300 steel were previously obtained by the Santos et al[25] in terms of the tensile strength and Young's modulus, hardness, and porosity.

TABLE 3 Fatigue testing program

Test	Material	R	ΔP, kN	ΔK_{BL}, MPa$\sqrt{m}$	OLR	No. of Overloads
Constant amplitude	SLM	0.05	2.63	-	-	-
	SLM + CK45	0.05	2.63	-	-	-
	SLM + AISI H13	0.05	2.63	-	-	-
	SLM + AISI 420	0.05	2.63	-	-	-
		0.3	2.26	-	-	-
		0.6	1.70	-	-	-
Overloads	SLM + CK45	0.05	2.63	12; 18	2	1
	SLM + AISI 420	0.05	2.63	12; 18	2	1; 10; 100

Fatigue crack growth tests were carried out under constant amplitude loading (ΔK increase) in order to study the stable crack growth in the Paris law regime. Figure 8 depicts da/dN-ΔK curves for the three hybrid specimens series with different conventional steels (AISI H13, or AISI 420, or CK45E), showing the influence of the substrate material for the stress ratio $R = 0.05$. The reference da/dN-ΔK curve obtained in this work for fully SLM samples, as well as crack propagation curves for the three substrate materials, taken from the literature,[26-28] was superimposed for comparison. The analysis of the figure shows a negligible influence of the substrate steel on the fatigue crack propagation over the entire ΔK range analysed. The main causes for these results are the site of crack initiation and the path of propagation. Figure 9 presents an exemplary and representative image of all fatigue tests, showing the crack initiation site and the propagation path in a sample with CK45 substrate. The analysis of this figure shows that crack initiated at the tip of the notch and propagated through the SLM material, within the layer near the interface, where the carbon migration occurred. As this layer has similar microstructure and chemical composition in all sample batches, and being the least resistant, it is the preferred region for crack growth.

The effect of mean stress on the da/dN-ΔK curves was studied for the samples with AISI420 steel substrate. The results for $R = 0.05$, 0.3, and 0.6 are plotted in Figure 10. Contrary to that observed in most conventional metals, a negligible effect of the mean stress was obtained in the

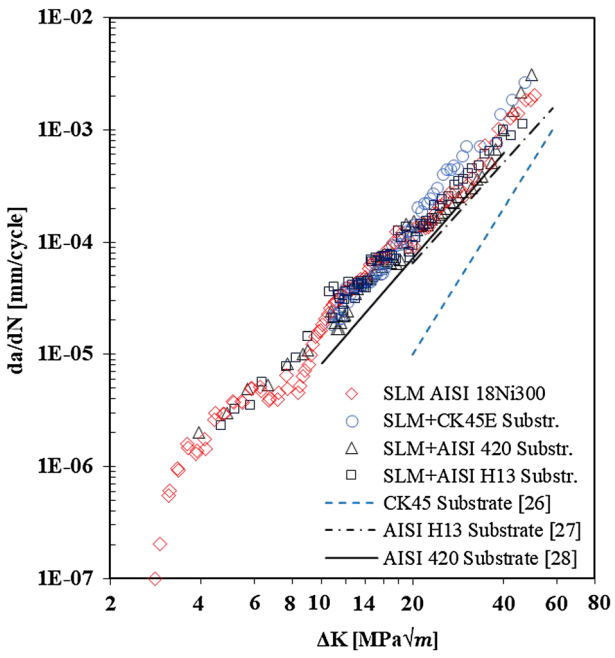

FIGURE 8 Comparison of da/dN-ΔK curves for SLM material, three different hybrid samples, and substrate materials[26-28]; $R = 0.05$ [Colour figure can be viewed at wileyonlinelibrary.com]

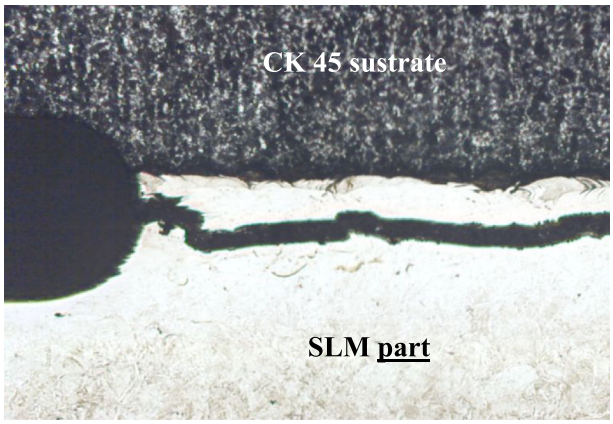

FIGURE 9 Fatigue crack initiation from the specimen notch tip. Hybrid specimen with CK45 substrate [Colour figure can be viewed at wileyonlinelibrary.com]

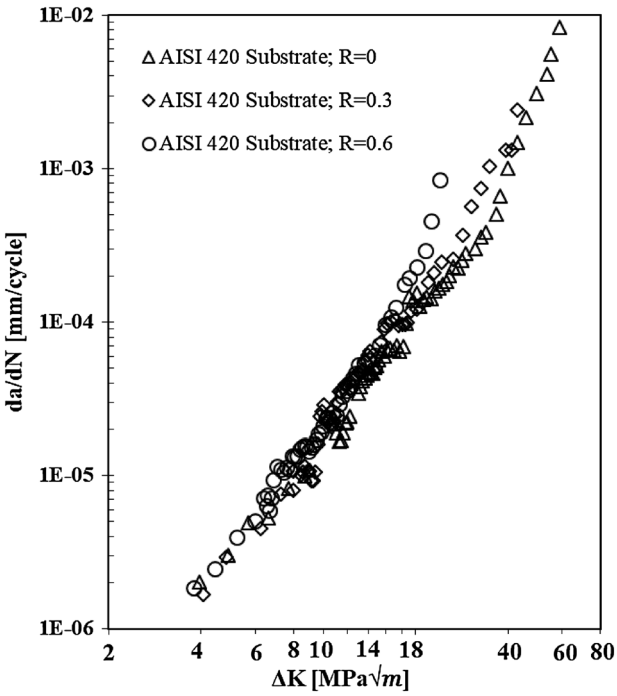

FIGURE 10 Effect of mean stress on the da/dN-ΔK curves of hybrid specimens with AISI420 steel substrate

Paris regime for SLM materials. Only in regime III, for the maximum K value approaching the fracture toughness of the material, a significant increase in crack growth rate with mean stress was observed.

For conventional metal materials, the fatigue crack growth is normally affected by mean stress, being this effect mainly caused by the plasticity at crack tip and consequently by crack closure.[19,29] Considering the reduced effect of the mean stress observed in Figure 10, the question arises whether this material produced by SLM exhibits crack closure.

To get answer to this question, the crack closure was monitored in all tests. As indicated previously, load-displacement curves were monitored at specific crack length intervals over each of the tests using the pin microgauge shown in Figure 3.

Opening loads, P_{op}, were derived from these records using the technique known as maximization of the correlation coefficient.[20] This technique involves taking the upper 10% of the load-displacement data (cycle loading phase) and calculating the least squares correlation coefficient. The next data pair is then added, and the correlation coefficient is again computed. This procedure is repeated for the whole data set. The point at which the correlation coefficient reaches a maximum can then be defined as P_{op}. Figure 11 shows one exemplary curve plotting the correlation coefficient against the load during the loading fatigue cycle phase. The analysis of the figure shows that a maximum on the correlation coefficient curve is not defined, this means no observance of the crack closure phenomena, which justify the reduced effect of the mean stress on the stable crack propagation regime.

As shown in Figure 9, the cracks started on the SLM material for all hybrid specimens and continue to propagate in this material near the interface with the substrate. Figure 12A,B shows the crack path for AISI420 and CK45 steel substrates, respectively, where cracks initially started from the notch in the SLM side. In all fatigue tests, the crack propagates in a zigzag path, showing mixed failure mode: transgranular with crack passing through the layer or interlayer failure, where the crack contours the deposited layers having steps of one, two, or three layers.

Table 4 summarizes the values of the Paris law constants obtained for the different hybrid samples tested under constant amplitude loading, considering da/dN in mm/cycle and ΔK in MPa$\sqrt{\text{m}}$.

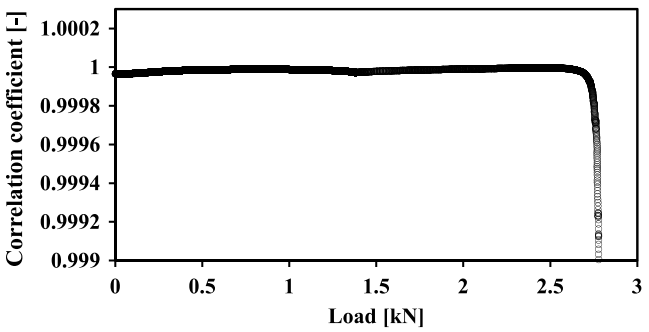

FIGURE 11 Opening load determination by the maximization of the correlation coefficient technique

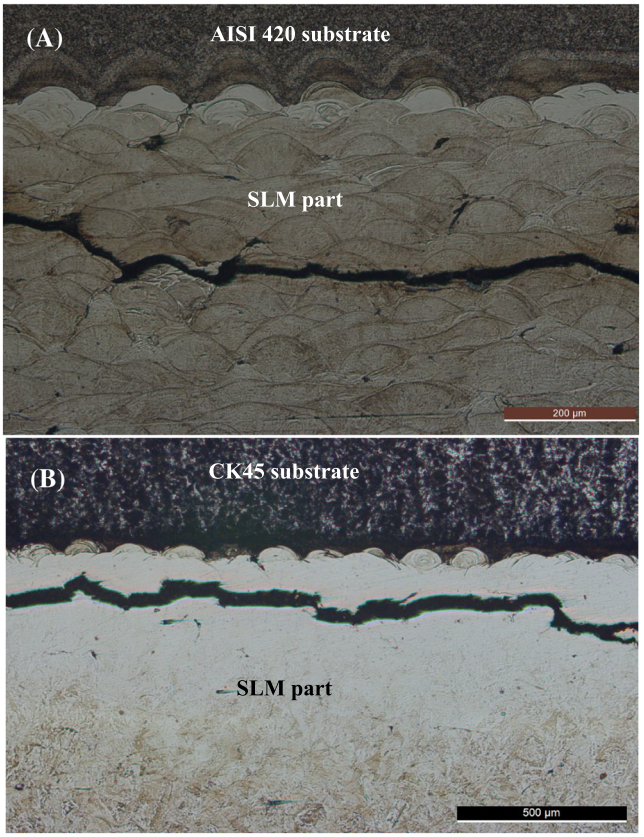

FIGURE 12 Crack path for hybrid samples: A, AISI 420 substrate; B, CK 45 substrate [Colour figure can be viewed at wileyonlinelibrary.com]

TABLE 4 Paris law parameters (da/dN in mm/cycle and ΔK in MPa$\sqrt{\text{m}}$)

Substrate Material	Stress Ratio R	C	m	Determination coefficient, R^2
Reference SLM material	0.05	4.218×10^{-8}	2.67	0.992
AISI H13	0.05	3.741×10^{-8}	2.71	0.989
CK45E	0.05	1.178×10^{-8}	3.30	0.981
AISI 420	0.05	4.606×10^{-8}	2.59	0.985
AISI 420	0.3	1.953×10^{-8}	2.64	0.979
AISI 420	0.6	2.132×10^{-8}	3.06	0.974

3.2 | Transient crack growth regime after overloading

The transient crack growth behaviour after the application of 1, 10, or 100 of tensile overloads applied at ΔK baseline levels of 12 and 18 MPa$\sqrt{\text{m}}$ with OLR = 2 was analysed. Figure 13A highlights the effect of the number of overloads on the da/dN-ΔK curves for samples with

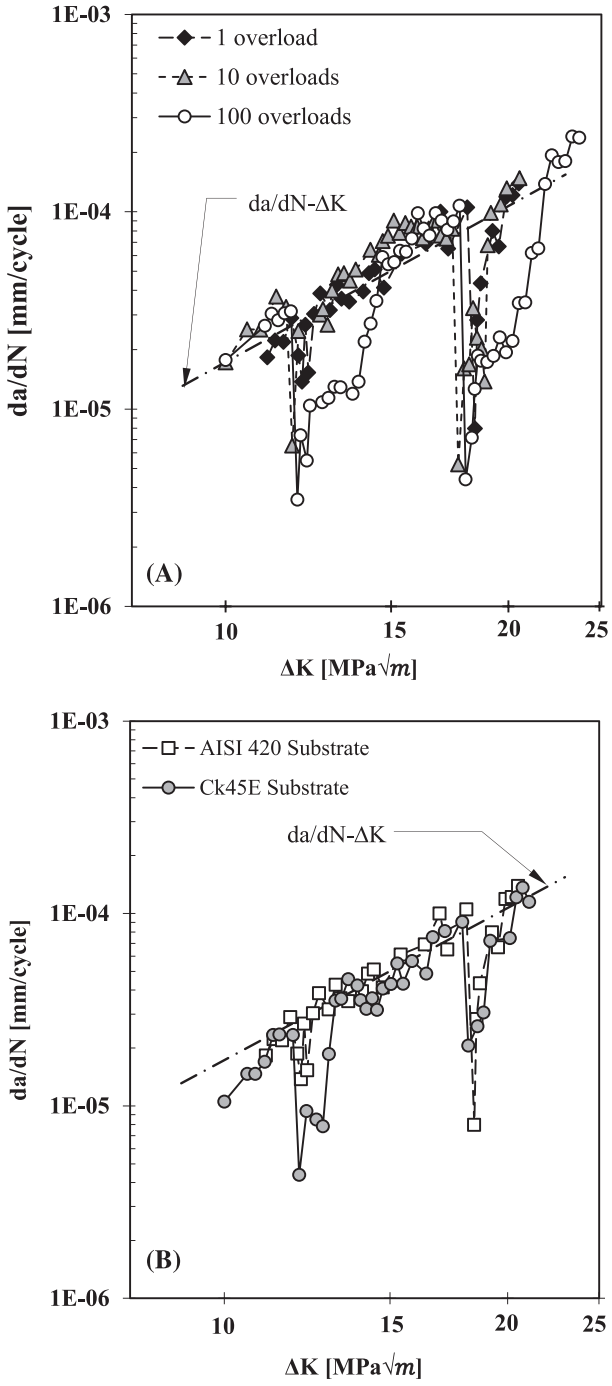

FIGURE 13 Transient regime due to overload application on hybrid samples: A, effect of the number of overloads for AISI 420 substrate; B, effect of the substrate with application of a single peak overload

AISI 420 steel substrate. For better comparison, the curve obtained under constant amplitude loading is superimposed in the figure. The results show the typical delay effect after overloading, which is normally reported in the literature for casting materials. This retardation is usually attributed to the crack closure effect.[19-23] However, despite the significant crack growth retardation induced by the overloads, crack closure was not observed in the present study, similarly to the depicted in Figure 11 . Figure 13A also shows that by increasing the number of overload cycles, the retardation effect increases significantly for both ΔK baseline values.

Figure 13B compares the transient propagation behaviour after application of a single peak overload in samples with CK45 and AISI 420 substrate steels. Both samples exhibit a very similar behaviour, which is once again due to the propagation of the crack occurring, in both cases, through SLM material close to the interface, similar to what was observed in constant load amplitude tests.

Failure surfaces were analysed in scanning electron microscope to identify the mechanisms of crack propagation. Figure 14A presents a representative image, obtained for a sample with CK45 substrate at a ΔK about 15 MPa$\sqrt{m}$, showing that brittle fracture is predominant. Figure 14B was also obtained for a sample with CK45 substrate after the application of an overload at a ΔK baseline level of 18 MPa$\sqrt{m}$, showing changes in the crack propagation plane and failure mode. The change of the crack path after the application of overloads is

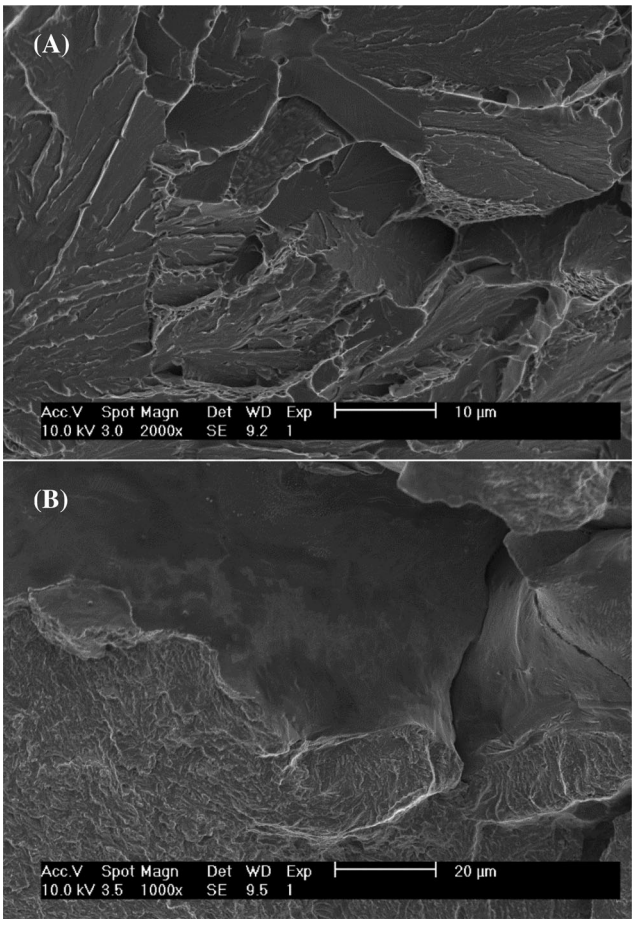

FIGURE 14 SEM observations of the surface failure on samples with CK45 substrate: A, stable crack growth; B, after a single tensile overload application at ΔK baseline of 18 MPa$\sqrt{m}$

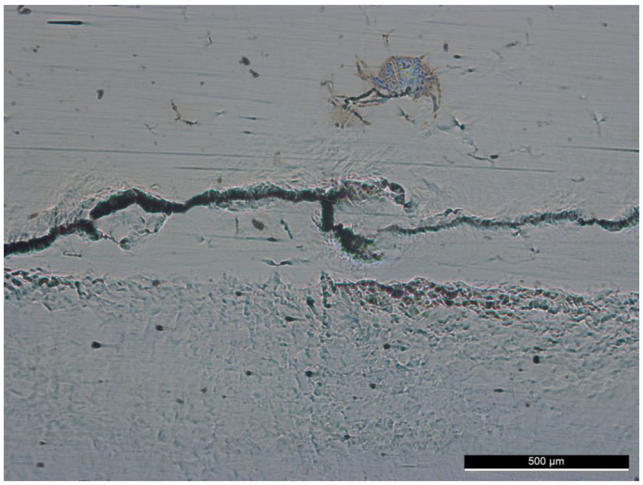

FIGURE 15 Crack bifurcation after overloading [Colour figure can be viewed at wileyonlinelibrary.com]

confirmed in Figure 15, which illustrates the respective crack bifurcation. The same figure also shows that cracks re-join after a transient period, and this behaviour is probably the main reason by the retardation observed in the fatigue crack propagation rate, despite the reduced crack closure phenomena observed in the SLM material.

4 | CONCLUSIONS

SLM and hybrid samples constituted by SLM material AISI 18Ni300 built on substrates in conventional steels were manufactured and tested in order to study the effect of substrate material and stress ratio on the fatigue crack propagation rate when subjected to constant amplitude loadings. The transient crack growth behaviour after overloads application was also investigated. The following conclusions can be drawn:

- Good fusion was achieved at the interface of the hybrid parts in all substrates, presenting a small level of defects and only some decarbonisation.
- The selective laser melting process induced longitudinal tensile residual stresses in near surface regions with an average value of about 220 MPa.
- The hardness and tensile strength of substrate steel has only a negligible effect on the fatigue crack propagation rate and on the crack path. Independent of the hardness of the substrate material, the fatigue failure occurs in the SLM material, near interface, at a distance between 150 and 200 μm.
- Fatigue crack retardation after single overload is very similar for all substrate materials. The study carried out did not detect the crack closure phenomena, being probably the retardation of the crack propagation due to the crack bifurcation observed after the overloads application.
- In agreement with the fact that crack closure was not observed, the mean stress produced only a reduced influence on the fatigue crack propagation rate under constant amplitude loading.

ACKNOWLEDGEMENTS

The authors would like to acknowledge the sponsoring under the project number 016713 (PTDC/EMS-PRO/1356/2014) financed by Project 3599 *Promover a Produção Científica e Desenvolvimento Tecnológico e a Constituição de Redes Temáticas* (3599-PPCDT) and FEDER funds and also EROFIO S.A. industry for the supply of the testing samples.

ORCID

Luis P. Borrego https://orcid.org/0000-0003-0259-8926

REFERENCES

1. Thompson SM, Bian L, Shamsaei N, Yadollahi A. An overview of direct laser deposition for additive manufacturing; part I: transport phenomena, modeling, and diagnostics. *Addit Manuf*. 2015;8:36-62.
2. Shamsaei N, Yadollahi A, Bian L, Thompson SM. An overview of direct laser deposition for additive manufacturing; part II: mechanical behavior, process parameter optimization and control. *Addit Manuf*. 2015;8:12-35.
3. Chan KS, Koike M, Mason RL, Okabe T. Fatigue life of titanium alloys fabricated by additive layer manufacturing techniques for dental implants. *Metall Mater Trans A*. 2013;44(2):1010-1022.
4. Wycisk E, Emmelmann C, Siddique S, Walther F. High cycle fatigue (HCF) performance of Ti-6Al-4V alloy processed by selective laser melting. *Adv Mat Res*. 2013;816:134-139.
5. Kasperovich G, Hausmann J. Improvement of fatigue resistance and ductility of TiAl6V4 processed by selective laser melting. *J Mater Process Technol*. 2015;220:202-214.
6. Leuders S, Thöne M, Riemer A, et al. On the mechanical behaviour of titanium alloy TiAl6V4 manufactured by selective laser melting: fatigue resistance and crack growth performance. *Int J Fatigue*. 2013;48:300-307.
7. Rafi HK, Starr TL, Stucker BE. A comparison of the tensile, fatigue, and fracture behavior of Ti-6Al-4V and 15-5 PH stainless steel parts made by selective laser melting. *Int J Adv Manuf Technol*. 2013;69(5-8):1299-1309.
8. Li P, Warner DH, Fatemi A, Phan N. Critical assessment of the fatigue performance of additively manufactured Ti-6Al-4V and perspective for future research. *Int J Fatigue*. 2016;85:130-143.
9. Rafi HK, Pal D, Patil N, Starr TL, Stucker BE. Microstructure and mechanical behavior of 17-4 precipitation hardenable steel processed by selective laser melting. *J Mater Eng Perform*. 2014;23(12):4421-4428.

10. Facchini L, Vicente N, Lonardelli I, Magalini E, Robotti P, Molinari A. Metastable austenite in 17-4 precipitation-hardening stainless steel produced by selective laser melting. *Adv Eng Mater*. 2010;12(3):184-188.
11. Luecke WE, Slotwinski JA. Stainless steel made by additive manufacturing. *J Res Natl Inst Stand Technol*. 2014;119:398-418.
12. Mower TM, Long MJ. Mechanical behavior of additive manufactured, powderbed laser-fused materials. *Mater Sci Eng A*. 2015;651:198-213.
13. Yadollahi A, Shamsaei N, Thompson SM, Elwany A, Bian L. Effects of building orientation and heat treatment on fatigue behavior of selective laser melted 17-4 PH stainless steel. *Int J Fatigue*. 2017;94(2):218-235.
14. Chawla N, Murphy TF, Narasimhan KS, Koopman M, Chawla KK. Axial fatigue behaviour of binder-treated versus diffusion alloyed powder metallurgy steels. *Mater Sci Eng A*. 2001;308(1-2):180-188.
15. D'Armas H, Llanes L, Penafiel J, Bas J, Anglada M. Tempering effects on the tensile response and fatigue life behaviour of a sinter-hardened steel. *Mater Sci Eng A*. 2000;277(1-2):291-296.
16. Carabajar S, Verdu C, Fougeres R. Damage mechanisms of a nickel alloyed sintered steel during tensile tests. *Mater Sci Eng A*. 1997;232(1-2):80-87.
17. Sudhakar KV. Fatigue behaviour of a high density powder metallurgy steel. *Int J Fatigue*. 2000;22(9):729-734.
18. Phillips RA, King JE, Moon JR. Fatigue crack propagation in some PM steels. *Powder Metall*. 2000;43(2):149-156.
19. Borrego LP, Ferreira JM, Costa JM. Fatigue crack growth and crack closure in an AlMgSi alloy. *Fatigue Fract Eng Mater Struct*. 2001;24(4):255-266.
20. Borrego LP, Ferreira JM, Costa JM. Evaluation of overload effects on fatigue crack growth and closure. *Eng Fract Mech*. 2003;70(11):1379-1397.
21. Borrego LP, Antunes FV, Costa JD, Ferreira JM. Numerical simulations of plasticity induced closure under overload and high-low blocks. *Eng Fract Mech*. 2012;95:57-71.
22. Borrego LP, Ferreira JM, Pinho da Cruz JM, Costa JM. Fatigue crack growth in thin aluminium alloy sheets under loading sequences with periodic overloads. *Thin-Wall Struct*. 2005;43(5):772-788.
23. Borrego LP, Ferreira JM, Costa JM. Partial crack closure under block loading. *Int J Fatigue*. 2008;30:1789-1796.
24. American Society for Testing and Materials. Standard test method for measurement of fatigue crack growth rates. Annual Book of ASTM Standards 2000: Volume 03.01, ASTM E 647.
25. Santos LMS, Ferreira JAM, Jesus JS, Costa JM, Capela C. Fatigue behaviour of selective laser melting steel components. *Theor Appl Fract Mech*. 2016;85:9-15.
26. Costa JDM, Ferreira JAM. Effect of stress ratio and specimen thickness on fatigue crack growth of the CK45 steel. *Theor Appl Fract Mech*. 1998;30(1):65-73.
27. Shah M, Ali M, Sultan A, et al. An investigation into the fatigue crack growth rate of electron beam-welded H13 tool steel: effect of welding and post-weld heat treatment. *Metallog Microstruc Anal*. 2014;3(2):114-125.
28. Plesiutschnig E, Fritzl P, Enzinger N, Sommitsch C. Fracture analysis of a low pressure steam turbine blade. *Case Studies Eng Fail Anal*. 2016;56:39-50.
29. Borrego LP, Costa JM, Antunes FV, Ferreira JM. Fatigue crack growth in aluminium alloys. *Eng Fail Anal*. 2010;17(1):11-18.

How to cite this article: Santos LMS, Ferreira JAM, Borrego LP, Costa JD, Capela C, de Jesus J. Fatigue crack propagation along interfaces of selective laser melting steel hybrid parts. *Fatigue Fract Eng Mater Struct*. 2019;42:2431–2440. https://doi.org/10.1111/ffe.13072